Mercury abundance and isotopic composition indicate subaerial volcanism prior to the end-Archean "whiff" of oxygen

Jana Meixnerová[1], Joel D. Blum[2,*], Marcus W. Johnson[2], Eva E. Stüeken[3,*], Michael A. Kipp[4], Ariel D. Anbar,[5], Roger Buick[1]

[1] Department of Earth and Space Sciences and Astrobiology Program, University of Washington, Seattle WA 98195-1310, USA
[2] Department of Earth and Environmental Sciences, University of Michigan, Ann Arbor MI 48109, USA
[3] School of Earth and Environmental Sciences, University of St Andrews, St Andrews Scotland KY16 9AL, UK
[4] Division of Geological and Planetary Sciences, California Institute of Technology, Pasadena CA 91125, USA
[5] School of Earth and Space Exploration and School of Molecular Sciences, Arizona State University, Tempe AZ 85287, USA
*Corresponding authors: jdblum@umich.edu, ees4@st-andrews.ac.uk

Significance

Earth's atmosphere became oxygenated around 2.4 billion years ago, and this event was preceded by at least one short-lived "whiff" of free O_2 gas nearly 100 million years earlier. The cause of this whiff has so far been difficult to identify. Here, we present mercury concentrations and isotope ratios across the whiff interval and find evidence for significant subaerial volcanism immediately preceding oxygenation. We propose that subaerial weathering of fresh volcanic rocks acted as a fertilizer that stimulated biological productivity and O_2 production in the surface ocean. Our results indicate another strong linkage between planetary magmatic processes and the evolution of Earth's atmosphere.

Abstract

Earth's early atmosphere witnessed multiple transient episodes of oxygenation before the Great Oxidation Event 2.4 billion years ago (Ga) [e.g., A. D. Anbar et al., *Science* 317, 1903–1906 (2007); M. C. Koehler, R. Buick, M. E. Barley, *Precambrian Res.* 320, 281–290 (2019)], but the triggers for these short-lived events are so far unknown. Here, we use mercury (Hg) abundance and stable isotope composition to investigate atmospheric evolution and its driving mechanisms across the well-studied "whiff" of O_2 recorded in the ~2.5-Ga Mt. McRae Shale from the Pilbara Craton in Western Australia [A. D. Anbar et al., *Science* 317, 1903–1906 (2007)]. Our data from the oxygenated interval show strong Hg enrichment paired with slightly negative Δ^{199}Hg and near-zero Δ^{200}Hg, suggestive of increased oxidative weathering. In contrast, slightly older beds, which were evidently deposited under an anoxic atmosphere in ferruginous waters [C. T. Reinhard, R. Raiswell, C. Scott, A. D. Anbar, T. W. Lyons, *Science* 326, 713–716 (2009)], show Hg enrichment coupled with positive Δ^{199}Hg and

slightly negative Δ^{200}Hg values. This pattern is consistent with photochemical reactions associated with subaerial volcanism under intense UV radiation. Our results therefore suggest that the whiff of O_2 was preceded by subaerial volcanism. The transient interval of O_2 accumulation may thus have been triggered by diminished volcanic O_2 sinks, followed by enhanced nutrient supply to the ocean from weathering of volcanic rocks causing increased biological productivity.

Introduction

The stepwise oxygenation of Earth's surface constituted a fundamental transformation of our planet's atmosphere. The mechanisms driving this transition are still debated. The most studied part of this transformation is the first permanent rise in atmospheric O_2, which occurred ~2.45 billion years ago (Ga), termed the "Great Oxidation Event" (GOE) ([1], [2]). However, geochemical records ([3]–[7]) point to biological O_2 production in localized environments as much as 500 My before the GOE. These transient "whiffs" of O_2, which are archived in pyritic, organic-rich mudstones that are commonly ascribed to high biological productivity and organic carbon burial in Archean "oxygen oases" ([8]), raise questions about what may have stimulated the early production of O_2 and buffered its atmospheric concentration.

Volcanism can play a central role in modulating both sources and sinks of O_2. For instance, the production of O_2 could be stimulated by the emplacement of large igneous provinces (LIPs) because weathering of fresh basaltic crust liberates the essential macronutrient phosphorus (P) ([9]), which is thought to ultimately modulate primary productivity over geologic time scales ([10]). The consumption of O_2 is also affected by volcanism because reaction with volcanic gases provides a long-term sink for atmospheric O_2 (e.g., ref. [11]), which might have diminished in strength over time ([12], [13]). Indeed, periods of Neoarchean subaerial volcanism roughly coincide with the hypothesized O_2 whiffs and accompanying euxinic (sulfide-rich) events ([14], [15]), but cause–effect relationships between these events are so far unclear.

Here, we set out to more precisely track the relationship between volcanism and whiffs of O_2 using mercury (Hg) geochemistry. Throughout Earth's history, volcanism has been the principal source of Hg to the environment. Therefore, elevated Hg concentrations in sediments have been proposed to indicate large subaerial volcanic eruptions ([16]). The emitted Hg(0) is highly volatile and can be transported globally during its relatively long present-day atmospheric residence time of up to ~2 y ([17]). Photo-oxidation of volcanically emitted gaseous Hg(0) creates highly reactive and water-soluble Hg(II), which is deposited in rainfall. Adsorption to organic matter or sulfide minerals can transfer this dissolved Hg into sediments ([18]). Since common modern Hg sources such as erosion of humic soils, forest fires, and coal combustion were absent before the evolution of land plants, Hg sources in the Archean were shallow submarine or subaerial volcanism, or oxidative weathering of Hg-bearing sulfide minerals on land ([19], [20]). The residence time of gaseous Hg(0) in the Archean atmosphere may have been longer in the absence of oxidants, or shorter in the presence of more intense photochemistry, but in any case, it is likely that an atmospheric Hg cycle, driven by volcanic emissions, existed in the Archean.

The stable isotopic composition of Hg has been increasingly used to illuminate the movement of Hg through the environment. Hg isotopes can undergo mass-dependent fractionation

(MDF) (δ^{202}Hg), mass-independent fractionation of the odd isotopes (odd-MIF) (Δ^{199}Hg and Δ^{201}Hg), and mass-independent fractionation of the even isotopes (even-MIF) (Δ^{200}Hg and Δ^{204}Hg). For brevity, the magnitude of odd-MIF is reported here as Δ^{199}Hg, and even-MIF as Δ^{200}Hg. While Hg-MDF is associated with most biotic and abiotic pathways of the Hg cycle, Hg even-MIF is limited to photochemical transformations of Hg in the tropopause or stratosphere, while Hg odd-MIF is limited to photochemical transformations in the troposphere and in surface waters ([18], [21]–[23]). In the Archean, in the absence of an ozone shield, the intensity and spatial distribution of UV-driven photochemistry may have been different from today, but previous work has shown that strong MIF effects associated with atmospheric Hg cycling were present at that time ([24]), and therefore Hg-MIF can help distinguish between subaerial and submarine volcanism as well as provide insights into atmospheric composition.

LIP events during the Phanerozoic appear to have released enormous amounts of Hg into the surface environment, creating significant Hg enrichments and isotopic excursions in the stratigraphic record that have been used in numerous studies to identify links between LIPs, ocean redox changes, and biotic turnover (reviewed in ref. [16]). Perhaps the best example is a shift of up to 0.2‰ in Δ^{199}Hg across the end-Permian mass extinction event, reflecting the emplacement of the Siberian Traps ([25]). These findings open up the tantalizing possibility of investigating similar linkages between volcanism and biogeochemical perturbations in the Neoarchean. Here, we present Hg isotope data across the well-studied ~2.5-Ga Mt. McRae Shale, which records the best-documented O_2 oxygenation episode prior to the GOE ([3], [7], [26]). We present data across the anoxic-oxic transition and consider their potential to constrain the driver(s) of the observed O_2 whiff.

Geological Setting

Our samples came from drill core ABDP-9 drilled in Caliwingina Creek at 21°59′29.5″S, 117°25′13.6″E (*SI Appendix*, Fig. S1), drill hole azimuth 186°, dip 89°. The Mount McRae Shale was deposited along the southern margin of the Pilbara craton ([27]) in a deep subtidal environment by hemipelagic sedimentation ([28]). It is about 100 m thick and is underlain by the Mt. Sylvia Formation and capped by the Dales Gorge Member of the Brockman Iron Formation. Anbar et al. ([3]) obtained an age of 2,501.1 ± 8.2 million years from Re/Os geochronology for the drill core ABDP-9; subsequent reanalysis by Kendall et al. ([29]) yielded two less precise but more methodologically sound dates of 2,495 ± 14 Ma for the 145- to 148-m interval and 2,495 ± 20 Ma for the 128- to 129-m interval. Rasmussen et al. ([30]) obtained a date of 2,504 ± 5 million years from U/Pb geochronometry of zircons in tuff from elsewhere in the Mt. McRae Shale, but the precise stratigraphic location within the formation was not reported. Rocks underlying the Mt. McRae Shale in the area of ABDP-9 have only been metamorphosed to prehnite-pumpellyite facies ([31]–[33]). Deformation has been limited to very gentle open folding and sparse formation of ~1-cm chlorite veins oriented parallel to bedding ([34]). Potential metasomatic effects on primary geochemical proxies distal to veins have previously been discounted; they are unlikely to have been significant, given the consistency between multiple redox indicators across the whiff interval ([29], [34]).

The Mt. McRae Shale in ABDP-9 extends from 105 to 190 m. The uppermost 20 m are characterized by interbedded calcitic carbonates and gray/black shale with pyrite sparsely present, gradually passing down into black shale with increasing pyrite. Pyrite nodules occur

in great abundance from 131 m to 134 m, underlain by a 15-m-thick section of black shale with frequent pyrite laminae and nodules. Below this section, pyrite content drops as the dominant lithology passes into laminated sideritic and ankeritic carbonates with black shale interbeds. Beneath 173-m depth, pyritic black shale becomes dominant again, with carbonate/marl interbeds occurring until the base of the Mt. McRae Shale. The core was sampled at ∼2-m intervals for high stratigraphic resolution. Sampling deliberately avoided pyrite nodules and laminae to avoid secondary concentrations of Hg in remobilized sulfide minerals. Sampling also avoided proximity to chlorite veins to minimize any potential metasomatic effects.

Results

High-resolution Hg chemostratigraphy (**Figs. 1** and **2**) reveals two distinct excursions in Hg concentrations in regions dominated by organic-rich, pyritic black shale, with maxima of 491 ng/g at 179.05 m and 1,593 ng/g at 141.47-m stratigraphic depth. We examined these two intervals from 190 to 168 m and from 153 to 125 m at high stratigraphic resolution (approximately two samples per meter). When normalized to traditional sequestration proxies (total organic carbon [TOC], total sulfur [TS], Al, Fe, and Mo), Hg/TOC (in nanograms/gram/weight percent) shows a notable increase in the lower interval with a local maximum of 122.1 at 173.5 m and 118.8 at 137.31 m. Hg/Fe and Hg/Mo show enrichments in the lower interval rising to 68.9 (ng/g/wt%) and 199.2 (ng/g/μg/g), respectively, between 177 and 179 m, while Hg/TS and Hg/Al do not change appreciably (*SI Appendix*, Fig. S2). In the upper interval, Hg/Mo remains at the base level while Hg/TS, Hg/Fe, and Hg/Al show enrichment and fluctuations. Phosphorus remains constant in the lower interval averaging ∼226 μg/g, then sharply spikes between 170 m and 160 m with a maximum of 790 μg/g, and is then followed by fluctuating values averaging 337.5 μg/g in the upper interval.

Discussion

The Upper Mt. McRae Shale: Evidence of Oxidative Weathering:

Several geochemical proxies in the organic-rich shale section from ∼125 m to ∼153 m have previously been interpreted as evidence of transient oxygenation of shallow waters above a euxinic wedge, linked to a pulse of oxidative continental weathering and elevated primary productivity along continental margins (**3**, **26**, **34**–**36**). The Mt. McRae Shale would thus preserve a local, basinal expression of this event. We found strong Hg enrichment in this interval, coincident with excursions in TOC and redox-sensitive Mo and Re. Hg has a high affinity for organic matter, which is thought to be the main control on Hg sequestration into sedimentary rocks over geologic time scales (**16**). The linear relationship between Hg and TOC in this upper interval (**Fig. 3**) indicates that Hg removal was controlled by this well-known process. While the high TOC levels are explicable by heightened productivity linked to the whiff, the concurrent enrichment of Hg relative to TOC requires that the Hg reservoir in seawater also increased, suggesting enhanced Hg input from other sources.

We note that Hg/Mo remained constant, and these two elements were strongly correlated (*SI Appendix*, Figs. S2 and S3). As Mo is preferentially sequestered into sediments in a sulfidic water column, this correlation may indicate that Hg sequestration was facilitated by the expansion of euxinic conditions during this interval (**35**). However, given that sulfur was

generally not an abundant constituent of Archean seawater ([37]) and the expansion of sulfidic conditions is therefore temporally anomalous, the covariance between Hg, Mo, and euxinia (i.e., sulfide) likely indicates that the supply of all three elements to the ocean became enhanced at this time.

Our isotopic data suggest that the most plausible mechanism for enhanced Hg input in this upper interval of the Mt. McRae Shale is either hydrothermal input or oxidative weathering of fresh crustal rocks, which typically display Δ^{199}Hg (and Δ^{201}Hg) values close to zero, consistent with our observations. Fresh crustal rock may also include volcanic ash and fallout from prior volcanic eruptions (see below). While we cannot rule out a hydrothermal contribution, the covariance of the Hg/TOC spike in the upper shale with Mo, Re, U, Se, N, and other redox-sensitive tracers ([3], [26], [29], [34], [36]) is suggestive of oxidative weathering as the major Hg source during this interval. Contemporaneous volcanic emission of volatile Hg(0) is an unlikely source of Hg in this part of the section, because Phanerozoic studies suggest that the isotopic signature of large-scale subaerial volcanism is a slightly positive Δ^{199}Hg resulting from the oxidation of volcanogenic Hg(0) in the atmosphere and subsequent direct atmospheric deposition of positive odd-MIF–bearing Hg(II) ([16]). It is therefore more likely that the muted odd Hg-MIF signal across this interval reflects the input of lithogenic Hg released from land by oxidative weathering of previously deposited volcanic rocks or volcanogenic sulfide minerals that were not exposed to photochemical processes in the atmosphere and that do not carry any significant Hg odd-MIF (therefore, Δ^{199}Hg = ~0‰). The Hg data thus further support the inference of a whiff of O_2 during this interval ([3]).

The Lower Mt. McRae Shale: Evidence of Volcanic Input:

In contrast to the whiff interval, the older and stratigraphically lower part of the Mt. McRae Shale lacks enrichments in redox-sensitive trace elements. This interval is believed to have been deposited under an anoxic atmosphere in ferruginous waters ([35]). The Hg enrichment observed at ~177 m amounts to only about a third of the Hg anomaly across the O_2 whiff, and although TOC shows a small peak as well (possibly linked to high productivity), Hg/TOC ratios are again enriched and the maximum Hg/TOC ratio is comparable to the whiff interval (**Figs. 1** and **2**). Moreover, Hg is notably enriched over Mo in this interval, indicating a decoupling from weathering-induced sulfate input and ensuing water column euxinia. Oxidative weathering of crustal sulfides can be excluded as a viable Hg source during the deposition of the lower shale, because there is no evidence of oxygenation in any other proxies ([3], [26], [34]–[36]). The only other significant source of Hg in the late Archean was volcanism, and so the peak in Hg/TOC ratios at 173.5 m likely corresponds to enhanced volcanic Hg input. If so, then the small peak in TOC is perhaps explicable by short-lived fertilization by P derived from volcanic ash.

Throughout the lower core interval, Δ^{199}Hg shows positive values consistent with a volcanic contribution ([16]). Specifically, it has been shown that photo-oxidation of fresh volcanogenic Hg(0) leads to initial atmospheric deposition of Hg(II) carrying a positive Δ^{199}Hg signature. The complementary negative Δ^{199}Hg is held in residual gaseous Hg(0). When volcanism ends, this residual Hg(0) also undergoes photo-oxidation and rains out, possibly more distal to the volcanic source. A long-lived positive Δ^{199}Hg signature in sediments thus requires continuous replenishment of the proximal atmospheric Hg pool by volcanism. The decrease in Δ^{199}Hg up-section may thus be explained by decreasing volcanic input to the atmosphere

proximal to the sampling site, such that the rainout of background volcanogenic Hg from more distal sources would have become progressively more dominant in the samples. This process would over time have shifted the sedimentary Δ^{199}Hg to more negative values and created the gradual diminution of odd-MIF that we observe up-section. Alternatively, it is conceivable that the decrease in Δ^{199}Hg represents the buildup of a UV-shielding haze ([24]) that diminished Hg photochemistry. We cannot exclude this possibility, but the decline in Hg/TOC ratios up-section in the lower shale points toward a diminution of Hg input, consistent with declining volcanism near the basin. Interestingly, the Hg enrichment in the lower core closely underlies a very large positive excursion in the mass-independent fractionation of sulfur (S-MIF) (Δ^{33}S, **Fig. 2**). S-MIF is thought to form by photochemical reactions of sulfur-containing volcanic gases in the atmosphere ([38]), which strongly supports the hypothesis of subaerial volcanic activity. We speculate that the short stratigraphic extent of the S-MIF peak compared to the Hg-MIF signal reflects injection of volcanic gases into higher atmospheric layers, leading to the production of distinct UV effects.

We note that our observations differ from slightly older Archean black shales from the Griqualand West basin in South Africa (2.65–2.5 Ga) ([24]), which show a short-lived collapse in Δ^{200}Hg and Δ^{199}Hg to near-zero relative to high positive background values in both parameters. In that case, the positive background in both Δ^{200}Hg and Δ^{199}Hg was interpreted as evidence of extensive photochemical destruction of Hg gases in the absence of an ozone shield, while the collapse in Hg-MIF was interpreted as an episode of enhanced organic haze production. In our dataset, Δ^{199}Hg is positive while Δ^{200}Hg is negative during the lower core section. The origin of Δ^{200}Hg is currently not well understood but is thought to be related to Hg(0) oxidation under UV light ([39]). In Phanerozoic atmospheric samples, it is usually positive ([18], [21]). The difference between these two Archean datasets suggests a different atmospheric state during the deposition of the Mt. McRae Shale, possibly related to more intense volcanic activity around the 173.5-m horizon where Hg/TOC ratios are highest.

The interpretation of a significant volcanic event around the Hg/TOC peak at 173.5 m is consistent with the duration of the Hg enrichment interval. The average sedimentation rate of the Mt. McRae Shale is estimated to be ~4.5 m/My ([3], [29], [40]), so our lower core interval (22 m thick) could have been deposited over ~4.9 My. However, the sedimentation rate of carbonate-bearing rocks is usually higher than that of shales, estimated in the Hamersley Group to be ~12 m/My ([40]), so our lower core interval showing Hg enrichment among ferroan carbonate/black shale couplets may have accumulated rather more rapidly, in less than half this time. This timing is in agreement with the average lifetime of LIPs, most of which span a 1- to 5-My interval (with a maximum lifetime up to 50 My) and in which single magma pulses may have lasted from a few hundred thousand years up to 1 My ([41]). The Hg/TOC ratios up to 122 are of similar magnitude as those attributed to LIP events during extinction episodes and ocean anoxic events in the Phanerozoic sedimentary record ([16]), which further strengthens our interpretation.

Subaerial volcanism preceding an O_2 whiff begs the question about causality: Did a volcanic episode trigger transient O_2 accumulation? We propose that the immediate aftermath of LIP activity may have facilitated oxygenation because 1) O_2 sinks diminished, and 2) nutrient supply increased as LIPs were subject to weathering. Initially, volcanism likely released reducing gases, such as CO or H_2S, that act as O_2 sinks. Such gas emissions are short-lived compared to the much longer effect of weathering fresh volcanic rock ([42]). The cessation of

intense volcanism would thus have switched off this kinetically rapid O_2 sink, thereby promoting O_2 accumulation ([12]). On longer time scales, weathering and mobilization of nutrients would have gained prominence and enhanced biological productivity through the whiff interval. Freshly emplaced basaltic crust is highly susceptible to chemical weathering and is able to release significant amounts of P. This basaltic P source has been invoked as a fertilization mechanism for the ocean later in Earth's history ([9]). As the Archean biosphere is thought to have been predominantly P-limited ([43], [44]), such a nutrient injection may have stimulated biological productivity and increased the rate of O_2 production. Consistent with this logic, our data reveal a conspicuous P spike following the Hg enrichment and elevated Hg/TOC ratios in the lower core and preceding the whiff of O_2 ([Fig. 1]). This P excursion coincides with a bed of ferroan carbonate, so P enrichment resulting from lithologic changes cannot be excluded, but enhanced P bioavailability following volcanism appears likely and warrants further scrutiny.

Conclusions

This study utilizes Hg abundance and isotopic data that support the existing narrative that a whiff of oxygen was recorded by the upper shale interval of the Mt. McRae Shale. Our data also provide insights into potential causes of this event. Preceding this transient surface oxygenation event, a stratigraphically lower and older section of the Mt. McRae Shale records a Hg/TOC anomaly and isotopic pattern that is strongly suggestive of subaerial volcanism under unfiltered UV radiation of a magnitude and duration comparable to Phanerozoic LIPs. We hypothesize that the weathering of these flood basalts may have delivered nutrients such as P to the ocean and promoted primary productivity and thus the whiff of oxygen in its aftermath. In support of this hypothesis, it is notable that TOC levels increase markedly (~10-fold) from 170 m to 145 m ([Fig. 1]), peaking where oxygenation proxies such as Mo and Hg abundance are highest. So, while saturation of oxygen sinks is often regarded as the primary cause of the GOE ([12]), it seems that in the case of this pre-GOE oxygenation event a contributing factor may have also been volcanic-sourced phosphorus fertilization of biogenic oxygen production. While the Mt. McRae Shale is only a regional, short-lived example of a linkage between volcanism and oxygenation, it is conceivable that this linkage operated also on a global, protracted scale in the run-up to the GOE.

Materials and Methods

We analyzed 44 samples that had previously been analyzed for S, Fe, Se, C, and N isotopes and some trace metals ([3], [6], [34⇓]–[36], [45], [46]). For each sample, a billet was cut (3 cm × 5 cm × 1 cm) from the drill core using a water-cooled diamond blade tile saw. The billets were then broken into <5-mm chips without metal contact and ground to <100 mesh in silicon nitride ball mill vials. Samples were prepared for Hg isotope analysis in 2007, and again in 2018, following protocols described in detail by Biswas et al. ([47]) and Blum and Johnson ([39]). Briefly, Hg was released from between 0.1 and 1.5 g of powdered rock sample by thermal decomposition in a two-stage tube-furnace, carried by gold-trap filtered O_2, and captured in an oxidizing solution of 1% $KMnO_4$ (wt/wt) in 10% H_2SO_4 (vol/vol). In 2007, the amounts of sample processed yielded 200–400 ng of Hg per preparation. Trap solutions were neutralized by addition of 30% hydroxylamine-hydrochloride (wt/vol) in accordance

with EPA Method 1631 (Rev. E) recommendations and measured for Hg content using gold-amalgamation cold vapor–atomic absorption spectrophotometry (MA2000). Samples were then made ready for isotope measurement by dilution with additional neutralized $KMnO_4$ solution so that multiple samples could be analyzed at the same run solution concentration. In 2018, smaller amounts of sample material were processed, which yielded 30–180 ng of Hg per preparation, and additional processing followed thermal decomposition and trap neutralization. Hg content of each trap solution was assessed by cold vapor atomic fluorescence spectroscopy (CVAFS) (RA-3320F Gold+; Nippon Instruments) and then purged into a smaller secondary oxidizing trap solution with the same chemical composition as the initial trap. Use of a secondary trap separates Hg from sample matrix residues liberated by thermal decomposition and carried into the initial trap, and also enables preconcentration of Hg into the smallest practical volume so that isotope measurements may be made with the highest precision possible. Verification of secondary trap Hg contents was made by CVAFS measurements, and, as in 2007, final dilutions to common run solution concentrations were made by addition of neutralized $KMnO_4$ solution.

Process yields for the isotope preparation thermal decomposition step relative to direct-combustion atomic absorption spectrophotometry (AAS) averaged 98% (±10%, 1SD). For samples subjected to additional processing average yield associated with the purging of samples into secondary traps, relative to amount of Hg trapped from thermal decomposition, was 99% (±1%, 1SD). Larger scatter of thermal decomposition yield results may be attributable to the much smaller amounts of material (~0.05 g) processed for THg determination by direct-combustion AAS. The approximately 10-fold larger amounts of material processed per sample for isotope measurement diminishes the likelihood that uneven distribution of Hg in pulverized sample material could influence a THg result. The total Hg process blank associated with sample and standard reference materials (SRMs) prepared for isotope analysis averaged 0.3 ng per preparation, which represents an average contribution of 0.5% (± 0.2%, 1SD) to sample or SRM Hg.

Measurements of Hg isotopes were performed with a Nu Plasma (Nu Instruments) multicollector inductively coupled plasma mass spectrometer at the University of Michigan and results are presented following recommendations of Blum and Bergquist ([23]). Hg was released by $SnCl_2$ reduction as a cold vapor from a gas–liquid separator of custom design and combined with Tl (National Institute of Standards and Technology [NIST] SRM997) aerosol delivered from an Aridus desolvating nebulizer (Teledyne CETAC Technologies). Each analysis consisted of 24 10-s measurements followed by washout to a low, stable background signal. Background signals were assessed with on-peak-zero (OPZ) measurements of neutralized $KMnO_4$ solution, which were subtracted from signals measured during the subsequent analysis. Instrumental mass-bias was accounted for by using both an exponential fractionation law applied to individual measurements of samples and SRMs, and strict sample-standard bracketing of samples with analyses of NIST SRM3133. Evaluation of potential isobaric interference with the measurement of ^{204}Hg was made by monitoring for any signal attributable to ^{206}Pb, which was never detected.

MDF of Hg isotopes is reported as δ^{202}Hg in permil (‰) relative to NIST SRM 3133 (**Eq. 1**). MIF of Hg isotopes is calculated as the difference between the measured δ^{202}Hg value and that which would be predicted based on mass dependence for a given isotope and is reported as Δ^{xxx}Hg in permil (**Eq. 2**), where xxx is the mass of each Hg isotope 199, 200, 201, and 204,

and β is the mass proportionality constant (0.2520, 0.5024, 0.7520, and 1.493, respectively) (23):

$$\delta^{202}\mathrm{Hg} = \left(\left(\frac{\left(\frac{202_{Hg}}{198_{Hg}} \right)_{sample}}{\left(\frac{202_{Hg}}{198_{Hg}} \right)_{NIST\ 3133}} \right) - 1 \right) \times 1000,$$

[1]

$$\Delta^{xxx}\mathrm{Hg} \approx \delta^{xxx} - \left(\delta^{202} \times \beta \right).$$

[2]

In 2007, limitations imposed by the available collector array made it impossible to simultaneously measure all seven stable Hg isotopes, the two Tl isotopes, and a Pb isotope. The default configuration only permitted measurement of consecutive Hg isotopes (^{198}Hg–^{202}Hg). A small subset of samples processed at that time were measured again during a second analytical session in which an alternate collector configuration enabled measurement of ^{198}Hg, ^{200}Hg–^{202}Hg, and ^{204}Hg, but not ^{199}Hg. Subsequent to the 2007 analyses, the collector array of the instrument was upgraded. Consequently, in 2018 simultaneous measurements were made for the full range of isotopes, from ^{196}Hg to ^{206}Pb.

For analyses performed in 2007, instrument sensitivity for Hg was 0.64 V/ppb (total beam) and OPZ measurements indicated that about 1% of sample or bracketing standard signals could be attributed to carryover from the preceding analysis. Subsequent modifications to the inlet system and instrument interface improved sensitivity and reduced potential carryover to the extent that in 2018 Hg sensitivity was 2.79 V/ppb with a measured blank contribution of about 0.1%.

Estimates of analytical uncertainty (*SI Appendix,* Table S1) for samples are the larger average 2SD of the following: measurements of multiple preparations of UM-Almaden and NIST3133 used as periodic performance checks during mass spectrometer sessions; and measurements of multiple-sample and SRM process replicate preparations (*SI Appendix,* Tables S2 and S3).

Data Availability

All study data are included in the article and/or supporting information.

Acknowledgments
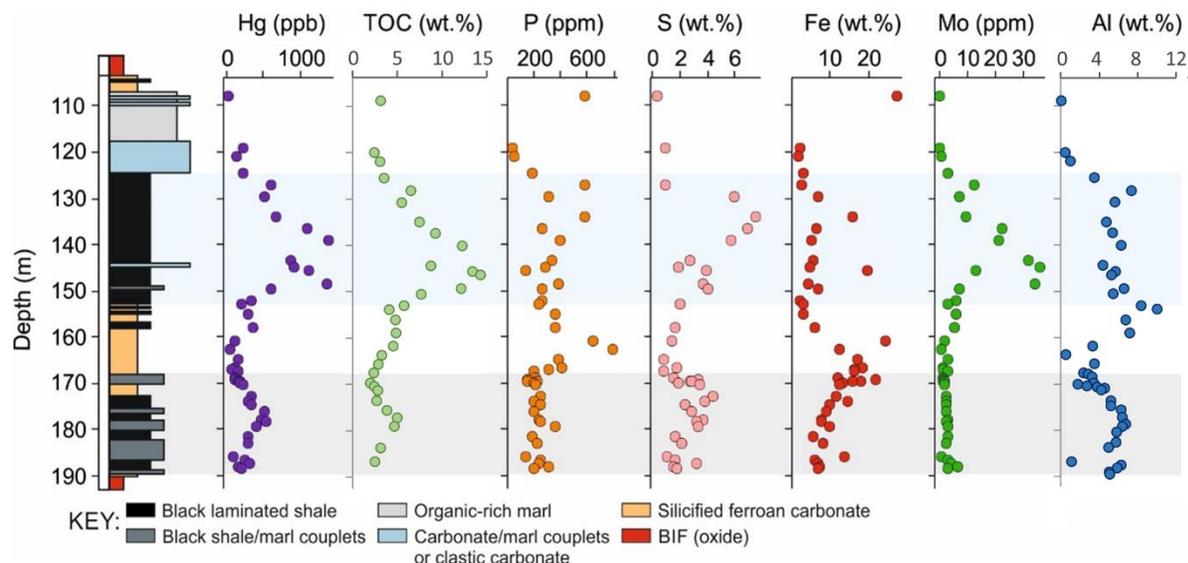
**Figure 1.** Lithology and chemostratigraphy of the Mt. McRae Shale. TOC, P, S and metal data were taken from the literature (1, 7). The gray and blue shaded areas respectively mark the lower and upper shale horizons showing Hg enrichments and isotopic excursions.
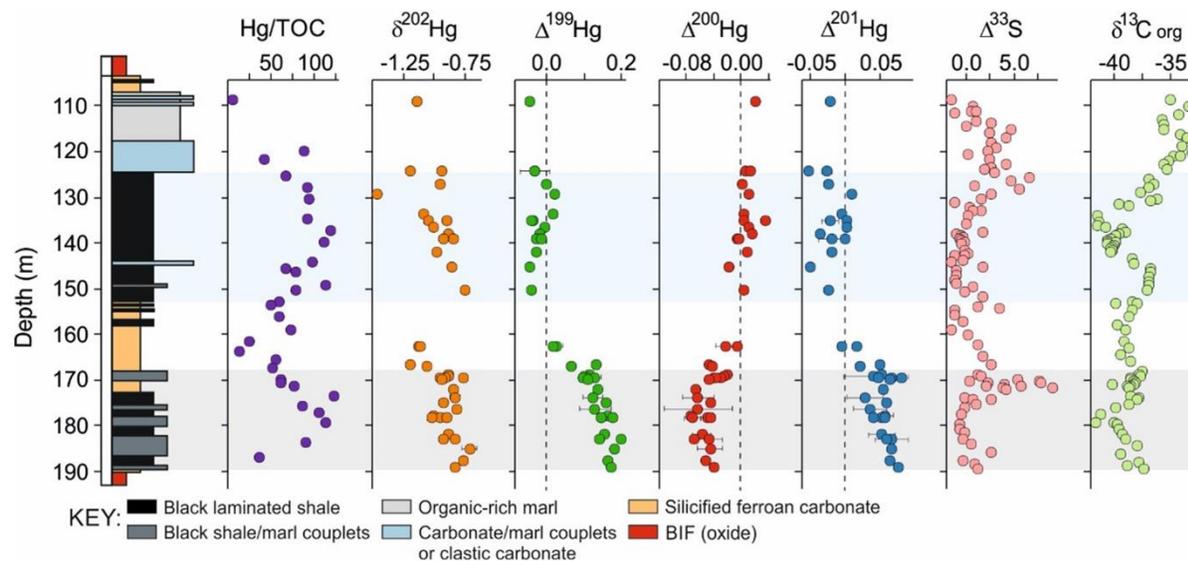
Figure 2. Lithology and isotopic chemostratigraphy of the Mt. McRae Shale. C and S isotopic data was taken from Kaufman et al. (2007) (7).
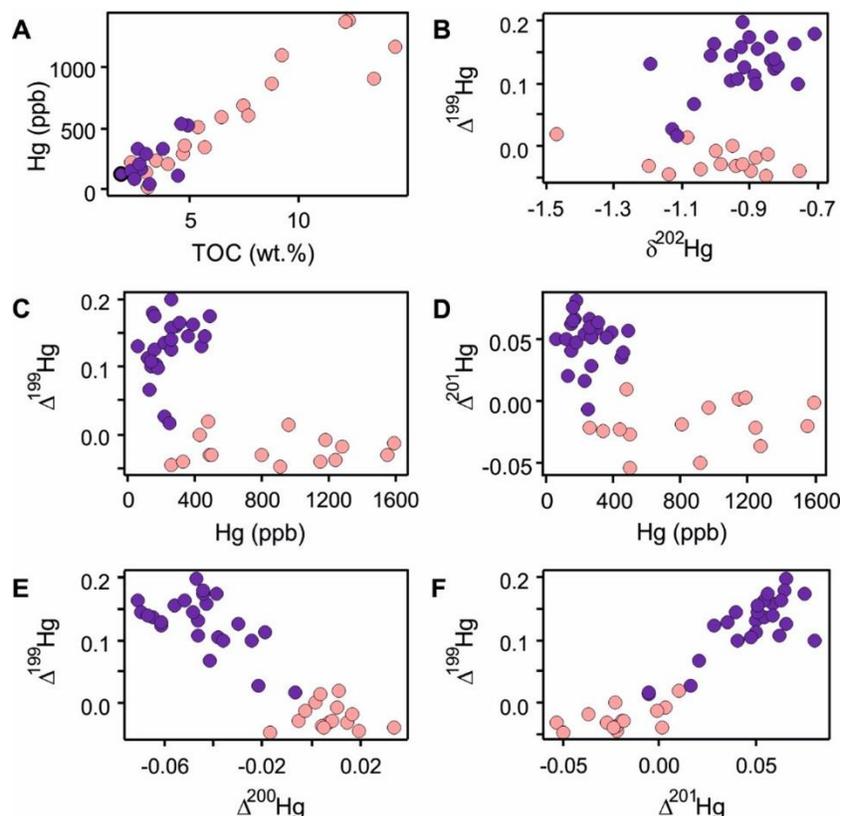
Figure 3. Cross plots of geochemical data. Dark purple data points correspond to the lower interval from 180 to 160 m stratigraphic depth, pink data points represent the upper interval above 160 m and include the 'whiff' of oxygen. Apart from Hg/TOC, elemental abundances and isotopes exhibit distinctly different relationships in the two sections of the core (also see Fig. S2).

Footnotes

- [1]To whom correspondence may be addressed: Email: jdblum@umich.edu or ees4@st-andrews.ac.uk.
- Author contributions: J.D.B., E.E.S., and A.D.A. designed research; J.M. performed research; J.D.B and M.W.J. contributed new reagents/analytic tools; J.D.B., M.W.J., E.E.S., M.A.K., A.D.A., and R.B. analyzed data; and J.M., J.D.B., E.E.S., M.A.K., A.D.A., and R.B. wrote the paper.
- Reviewers: J.F., University of Maryland, College Park; T.M.J., University of Illinois at Urbana–Champaign; and L.R.K., Pennsylvania State University.
- The authors declare no competing interests

References

1.   Warke MR, *et al.* (2020) The Great Oxidation Event preceded a Paleoproterozoic "Snowball Earth". *Proceedings of the National Academy of Sciences* 117:13314-13320.

2.   Holland, H. (2006) The oxygenation of the atmosphere and oceans. *Philosophical Transactions of the Royal Society B: Biological Sciences* 361, 903–915.

3.   Anbar A*, et al.* (2007) A whiff of oxygen before the Great Oxidation Event? *Science* 317(5846):1903-1906.

4.   Koehler MC, Buick R, Kipp MA, Stüeken EE, & Zaloumis J (2018) Transient surface oxygenation recorded in the ~2.66 Ga Jeerinah Formation, Australia. *Proceedings of the National Academy of Sciences* 115:7711-7716.

5.   Kendall B*, et al.* (2010) Pervasive oxygenation along late Archaean ocean margins. *Nature Geoscience* 3:647-652.

6.   Kaufman AJ*, et al.* (2007) Late Archean biospheric oxygenation and atmospheric evolution. *Science* 317:1900-1903.

7.   Ostrander CM, Johnson AC, & Anbar AD (2021) Earth's First Redox Revolution. *Annual Review of Earth and Planetary Sciences* 49:doi: 10.1146/annurev-earth-072020-055249.

8.   Olson SL, Kump LR, & Kasting JF (2013) Quantifying the areal extent and dissolved oxygen concentrations of Archean oxygen oases. *Chemical Geology* 362:35-43.

9.   Horton F (2015) Did phosphorus derived from the weathering of large igneous provinces fertilize the Neoproterozoic ocean? *Geochemistry, Geophysics, Geosystems* 16(6):1723-1738.

10.   Tyrrell T (1998) The relative influences of nitrogen and phosphorus on oceanic primary production. *Nature* 400:525-531.

11.   Holland HD (2002) Volcanic gases, black smokers, and the Great Oxidation Event. *Geochimica et Cosmochimica Acta* 66(21):3811-3826.

12.   Kadoya S, Catling DC, Nicklas RW, Puchtel IS, & Anbar AD (2020) Mantle data imply a decline of oxidizable gases could have triggered the Great Oxidation. *Nature Communications* 11:2774.

13.   Aulbach S & Stagno V (2016) Evidence for a reducing Archean ambient mantle and its effects on the carbon cycle. *Geology* 44(9):751-754.

14.   Prokoph A, Ernst RE, & Buchan KL (2004) Time-series analysis of large igneous provinces: 3500 Ma to present. *The Journal of Geology* 112(1):1-22.

15.   Kump LR & Barley ME (2007) Increased subaerial volcanism and the rise of atmospheric oxygen 2.5 billion years ago. *Nature* 448(7157):1033-1036.

16.   Grasby SE, Them II TR, Chen Z, Yin R, & Ardakani OH (2019) Mercury as a proxy for volcanic emissions in the geologic record. *Earth-Science Reviews* 196:102880.

17.   Sanei H, Grasby SE, & Beauchamp B (2012) Latest Permian mercury anomalies. *Geology* 40(1):63-66.

18.   Blum JD, Sherman LS, & Johnson MW (2014) Mercury isotopes in earth and environmental sciences. *Annual Review of Earth and Planetary Sciences* 42:249-269.

19.   Bergquist BA (2017) Mercury, volcanism, and mass extinctions. *Proceedings of the National Academy of Sciences* 114(33):8675-8677.

20.   Thibodeau AM & Bergquist BA (2017) Do mercury isotopes record the signature of massive volcanism in marine sedimentary records? *Geology* 45(1):95-96.

21.   Chen J, Hintelmann H, Feng X, & Dimock B (2012) Unusual fractionation of both odd and even mercury isotopes in precipitation from Peterborough, ON, Canada. *Geochimica et Cosmochimica Acta* 90:33-46.

22. Bergquist BA & Blum JD (2009) The odds and evens of mercury isotopes: applications of mass-dependent and mass-independent isotope fractionation. *Elements* 5(6):353-357.
23. Blum JD & Bergquist BA (2007) Reporting of variations in the natural isotopic composition of mercury. *Analytical and Bioanalytical Chemistry* 388:353-359.
24. Zerkle AL*, et al.* (2020) Anomalous fractionation of mercury isotopes in the Late Archean atmosphere. *Nature Communications* 11(1):1-9.
25. Grasby SE*, et al.* (2017) Isotopic signatures of mercury contamination in latest Permian oceans. *Geology* 45(1):55-58.
26. Ostrander CM*, et al.* (2019) Fully oxygenated water columns over continental shelves before the Great Oxidation Event. *Nature Geoscience* 12(3):186-191.
27. Blake TS & Barley ME (1992) Tectonic evolution of the late Archaean to early Proterozoic Mount Bruce Megasequence set, Western Australia. *Tectonics* 11(6):1415-1425.
28. Krapež B, Barley ME, & Pickard AL (2003) Hydrothermal and resedimented origins of the precursor sediments to banded iron formation: sedimentological evidence from the Early Palaeoproterozoic Brockman Supersequence of Western Australia. *Sedimentology* 50(5):979-1011.
29. Kendall B, Creaser RA, Reinhard CT, Lyons TW, & Anbar AD (2015) Transient episodes of mild environmental oxygenation and oxidative continental weathering during the late Archean. *Science Advances* 1(10):DOI: 10.1126/sciadv.1500777
30. Rasmussen B, Blake TS, & Fletcher IR (2005) U-Pb zircon age constraints on the Hamersley spherule beds: Evidence for a single 2.63 Ga Jeerinah-Carawine impact ejecta layer *Geology* 33(9):725-728.
31. Smith RE, Perdrix JL, & Parks TC (1982) Burial metamorphism in the Hamersley Basin, Western Australia. *Australian Journal of Petrology* 23:75-102.
32. White AJR, Legras M, Smith RE, & Nadoll P (2014) Deformation-driven, regional-scale metasomatism in the Hamersley Basin, Western Australia. *Journal of Metamorphic Petrology* 32:417-433.
33. White AJR, Smith RE, Nadoll P, & Legras M (2014) Regional-scale metasomatism in the Fortescue Group volcanis, Hamersley Basin, Western Australia: implications for hydrothermal ore systems. *Journal of Petrology* 55(5):977-1009.
34. Stüeken EE, Buick R, & Anbar AD (2015) Selenium isotopes support free O_2 in the latest Archean. *Geology* 43(3):259-262.
35. Reinhard CT, Raiswell R, Scott CT, Anbar A, & Lyons TW (2009) A late Archean sulfidic sea stimulated by early oxidative weathering of the continents. *Science* 326:713-716.
36. Garvin J, Buick R, Anbar AD, Arnold GL, & Kaufman AJ (2009) Isotopic evidence for an aerobic nitrogen cycle in the latest Archean. *Science* 323:1045-1048.
37. Crowe SA*, et al.* (2014) Sulfate was a trace constituent of Archean seawater. *Science* 346(6210):735-739.
38. Farquhar J, Bao H, & Thiemens MH (2000) Atmospheric influence of Earth's earliest sulfur cycle. *Science* 289:756-758.
39. Blum JD & Johnson MW (2017) Recent developments in mercury stable isotope analysis. *Reviews in Mineralogy and Geochemistry* 82(1):733-757.

40. Trendall AF, Compston W, Nelson DR, De Laeter JR, & Bennett VC (2004) SHRIMP zircon ages constraining the depositional chronology of the Hamersley Group, Western Australia. *Australian Journal of Earth Sciences* 51(5):621-644.
41. Self S, Schmidt A, & Mather TA (2014) Emplacement characteristics, time scales, and volcanic gas release rates of continental flood basalt eruptions on Earth. *Geological Society of America Special Papers* 505:319-337.
42. Jones MT, Jerram DA, Svensen HH, & Grove C (2016) The effects of large igneous provinces on the global carbon and sulphur cycles. *Palaeogeography, Palaeoclimatology, Palaeoecology* 441:4-21.
43. Kipp MA & Stüeken EE (2017) Biomass recycling and Earth's early phosphorus cycle. *Science Advances* 3(11):doi: 10.1126/sciadv.aao4795.
44. Reinhard CT, *et al.* (2017) Evolution of the global phosphorus cycle. *Nature* 541(7637):386-389.
45. Duan Y, *et al.* (2010) Molybdenum isotope evidence for mild environmental oxygenation before the Great Oxidation Event. *Geochimica et Cosmochimica Acta* 74(23):6655-6668.
46. Kendall B, Brennecka GA, Weyer S, & Anbar AD (2013) Uranium isotope fractionation suggests oxidative uranium mobilization at 2.50 Ga. *Chemical Geology* 362:105-114.
47. Biswas A, Blum JD, Bergquist BA, Keeler GJ, & Xie Z (2008) Natural mercury isotope variation in coal deposits and organic soils. *Environmental Science & Technology* 42:8303-8309.

Supplementary Information for:

Mercury abundances and isotopic ratios indicate subaerial volcanism prior to the end-Archean "whiff" of oxygen

Jana Meixnerova et al.

Table S1. Analytical uncertainty estimates.

Material	Year	n Preparations	Average 2SD (‰)				
			δ202	Δ199	Δ200	Δ201	Δ204
Almaden and NIST3133	2007	10	0.06	0.03	0.03	0.02	
Almaden and NIST3133	2018	4	0.04	0.01	0.01	0.01	0.02
Process Replicates*	2007	6	0.21	0.03	0.03	0.05	
Process Replicates*	2018	4	0.05	0.02	0.02	0.01	0.01

*The 2007 process replicates include 2 preparations each of 5 ABDP-9 samples and NIST SRM1944. The 2018 replicates include preparations of 2 additional ABDP-9 samples, NIST SRM2711, and the NRC SRM MESS-3. Hg isotope results for reference materials are presented in Table S2 and results for ABDP-9 samples are presented in Table S3.

Table S2. Hg isotope results for SRMs. Values are ‰ relative to NIST SRM3133.

Material	n Preparations	Year Processed	δ202	2SD	Δ199	2SD	Δ200	2SD	Δ201	2SD	Δ204	2SD
UM-Almaden	5	2007	-0.56	0.08	-0.04	0.04	-0.01	0.04	-0.05	0.02	-0.03	
	2	2018	-0.54	0.03	-0.02	0.004	0.01	0.01	-0.04	0.01	0.00	0.01
NIST SRM3133	5	2007	0.00	0.03	0.00	0.02	0.00	0.02	0.00	0.01	-0.01	
	2	2018	0.00	0.04	0.00	0.02	0.00	0.01	-0.01	0.01	0.00	0.04
NIST SRM1944	4	2007	-0.34	0.42	-0.02	0.05	0.01	0.03	-0.02	0.02	0.04	
NIST SRM2711	2	2018	-0.22	0.02	-0.23	0.02	0.00	0.01	-0.19	0.004	0.01	0.003
MESS-3	2	2018	-2.11	0.05	0.00	0.01	0.01	0.03	-0.04	0.01	0.01	0.03

Table S3. Hg isotope results for ABDP-9 samples. Values are ‰ relative to NIST SRM3133. Replicate results used in estimation of analytical uncertainty for Table S1 are in bold and outlined in red.

Core Depth (m)	DC-AAS Hg (ng/g)	Isotope Prep Hg (ng/g)	Year Processed	Run-Solution Hg (ng/g)	δ202	2SD	Δ199	2SD	Δ200	2SD	Δ201	2SD	Δ204	2SD	Notes
112.52	313	261	2007	7	-1.14		-0.05		0.02		-0.02				
127.25	449	501	2007	10	-0.94		-0.03		0.01		-0.05				
127.25		495	2018	5	-1.20		-0.03		0.01		-0.03		-0.01		
130.06	496	437	2007	8	-0.95		0.00		0.00		-0.02				
132.13	518	534	2007	8	-1.23		0.02		0.00		-0.01				Process Replicate Re-run for [204]Hg
		427	2007	8	-1.66		0.02		0.02		0.02				
			2007	8	-1.52				0.01		0.02		0.00		
Avg. 132.13		**480**	**2007**		**-1.47**	**0.44**	**0.02**	**0.01**	**0.01**	**0.02**	**0.01**	**0.03**	**0.00**		
136.15	899	962	2007	8	-1.09		0.01		0.00		-0.01				
137.68	1205	1150	2007	8	-0.90		-0.04		0.03		0.00				
137.68		1245	2018	5	-1.05		-0.04		0.00		-0.02		0.00		
139.01	1145	1184	2007	8	-1.00		-0.01		0.01		0.00		-0.07		
140.25	1266	1286	2007	8	-0.85		-0.02		0.00		-0.01				Process Replicate Re-run for [204]Hg
		1275	2007	8	-0.93		-0.02		0.03		-0.05				
			2007	8	-0.87				0.03		-0.04		-0.06		
Avg. 140.25		**1280**	**2007**		**-0.88**	**0.08**	**-0.02**	**0.001**	**0.02**	**0.04**	**-0.04**	**0.04**	**-0.06**		
141.47	1552	1522	2007	7	-0.93		-0.01		0.00		0.01				Process Replicate Re-run for [204]Hg
		1664	2007	8	-0.84		-0.01		-0.01		0.00				
			2007	8	-0.77				0.00		-0.01		0.02		
Avg. 141.47		**1593**	**2007**		**-0.85**	**0.16**	**-0.01**	**0.005**	**0.00**	**0.01**	**0.00**	**0.02**	**0.02**		
141.47		1552	2018	5	-0.92		-0.03		-0.01		-0.02		0.01		
144.36	777	751	2007	7	-1.04		0.00		0.01		0.00				Process Replicate Re-run for [204]Hg
		856	2007	8	-0.98		-0.06		0.00		-0.06				
			2007	8	-0.93				0.02		0.01		0.02		
Avg. 144.36		**803**	**2007**		**-0.98**	**0.11**	**-0.03**	**0.10**	**0.01**	**0.03**	**-0.02**	**0.07**	**0.02**		
147.30	841	915	2007	7	-0.85		-0.05		-0.02		-0.05				
152.08	379	335	2007	8	-0.75		-0.04		0.00		-0.02				

163.95	239	250	2007	7	-1.11		0.02		-0.01		-0.01				
163.95		226	2018	5	-1.13		0.03		-0.02		0.02		0.05		
167.76	60	60	2018	5	-1.19		0.13		-0.05		0.05		0.05		
168.36	166	131	2018	5	-1.06		0.07		-0.04		0.02		0.09		
169.94	110	122	2018	5	-0.89		0.11		-0.02		0.05		0.04		
170.39	149	147	2018	5	-0.88		0.10		-0.02		0.04		0.07		
170.55	183	182	2007	10	-0.76		0.10		-0.04		0.08				
170.55		168	2018	5	-0.92		0.13		-0.03		0.07		0.08		
170.55*	175	174	2018	5	-0.96		0.10		-0.04		0.05		0.09		Process Replicate
Avg. 170.55		171	2018		-0.94	0.06	0.11	0.03	-0.03	0.01	0.06	0.03	0.08	0.01	
170.86	171	149	2018	5	-0.94		0.11		-0.05		0.06		0.08		
173.09	195	224	2007	10	-0.84		0.14		-0.07		0.05				
174.67	300	267	2018	5	-0.83		0.12		-0.06		0.03		0.08		
175.81	257	296	2007	10	-0.92		0.16		-0.04		0.06				
177.10	524	447	2018	5	-0.82		0.13		-0.06		0.04		0.12		
178.61	472	390	2018	5	-1.00		0.16		-0.07		0.06		0.09		
179.05	440	491	2007	8	-0.90		0.18		-0.04		0.06				
179.05		362	2018	5	-0.96		0.14		-0.05		0.05		0.13		
179.05*	534	459	2018	5	-1.01		0.15		-0.07		0.04		0.13		Process Replicate
Avg. 179.05		410	2018		-0.99	0.08	0.15	0.003	-0.06	0.03	0.05	0.02	0.13	0.01	
182.50	286	267	2018	5	-0.88		0.16		-0.06		0.05		0.09		
183.65	258	262	2007	7	-0.83		0.14		-0.07		0.06				
183.65		259	2018	5	-0.92		0.20		-0.05		0.07		0.14		
185.43	90	156	2018	5	-0.71		0.18		-0.04		0.07		0.12		
188.01	301	315	2007	7	-0.80		0.17		-0.07		0.03				
		305	2007	8	-0.74		0.16		-0.03		0.12				Process Replicate
			2007	8	-0.76				-0.05		0.05		0.08		Re-run for ^{204}Hg
Avg. 188.01		310	2007		-0.77	0.05	0.16	0.01	-0.05	0.04	0.06	0.10	0.08		
189.39	203	164	2018	5	-0.84		0.17		-0.04		0.08		0.11		

* denotes separate aliquot of powdered material provided for the 2018 analyses.
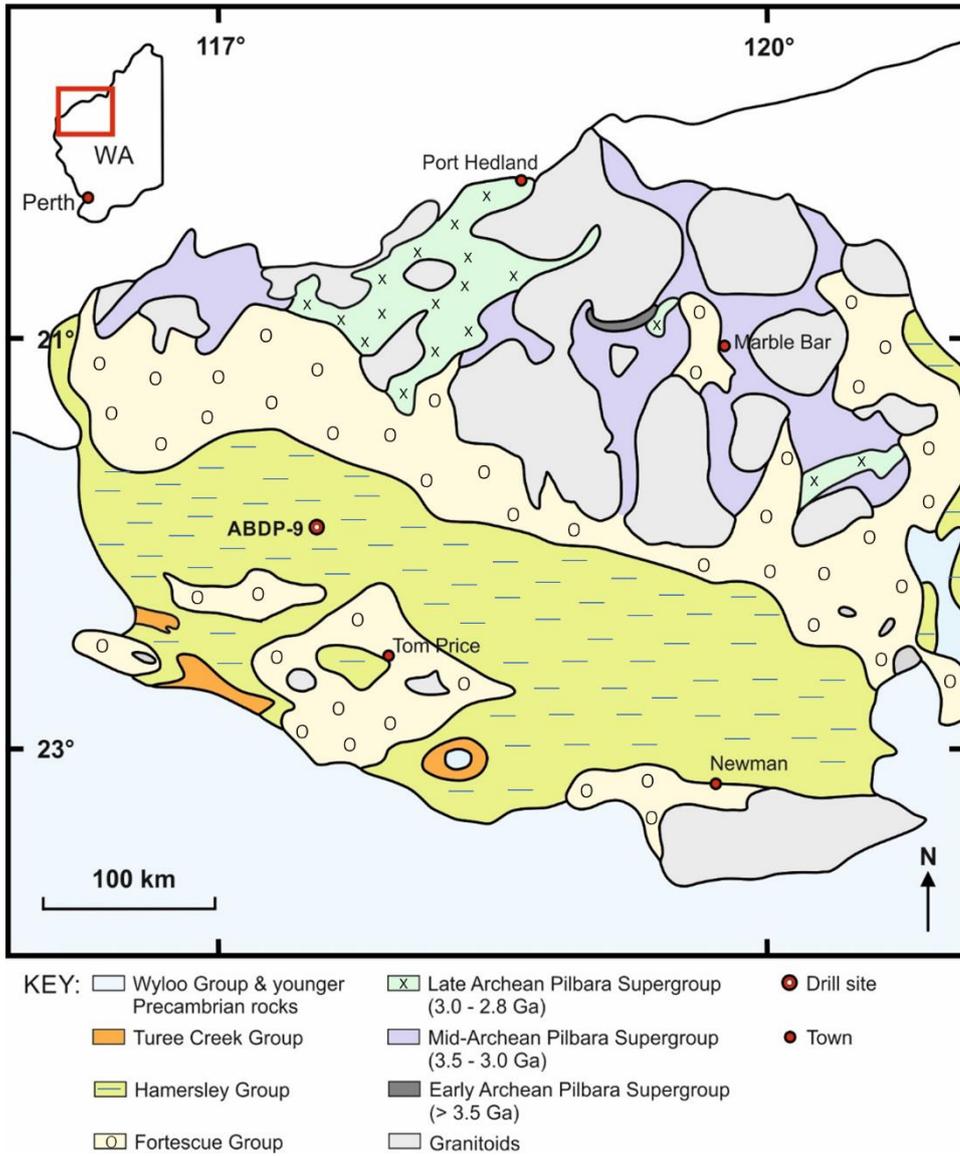
**Figure S1.** Geological context of the studied drill core.
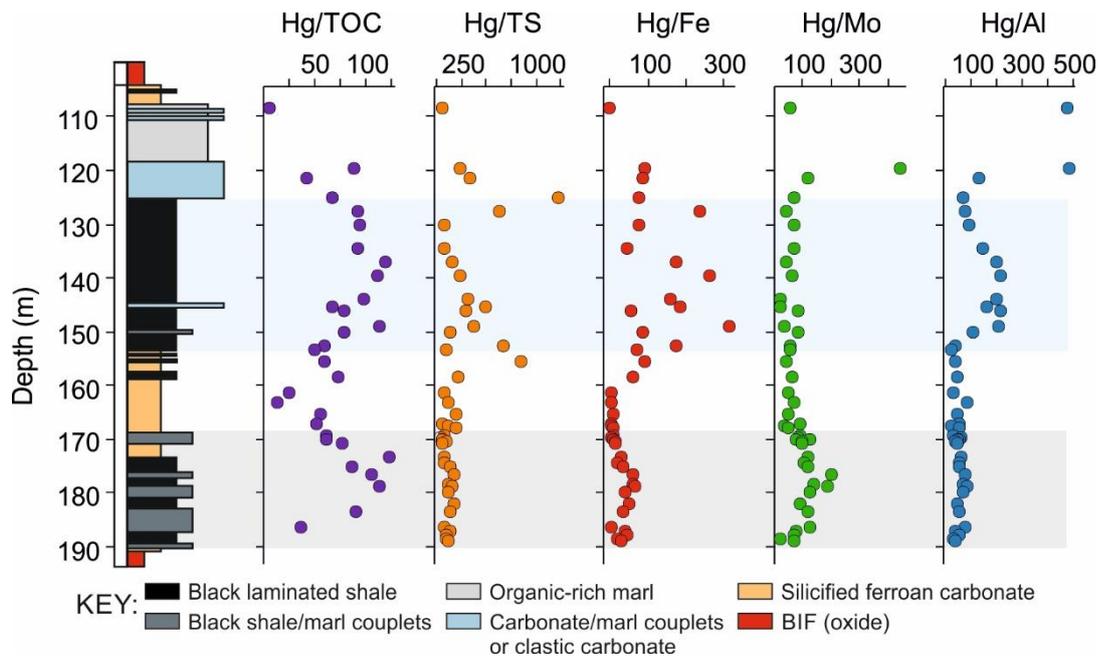
**Figure S2**. Selected diagnostic elements normalized to mercury across the Mt. McRae Shale.
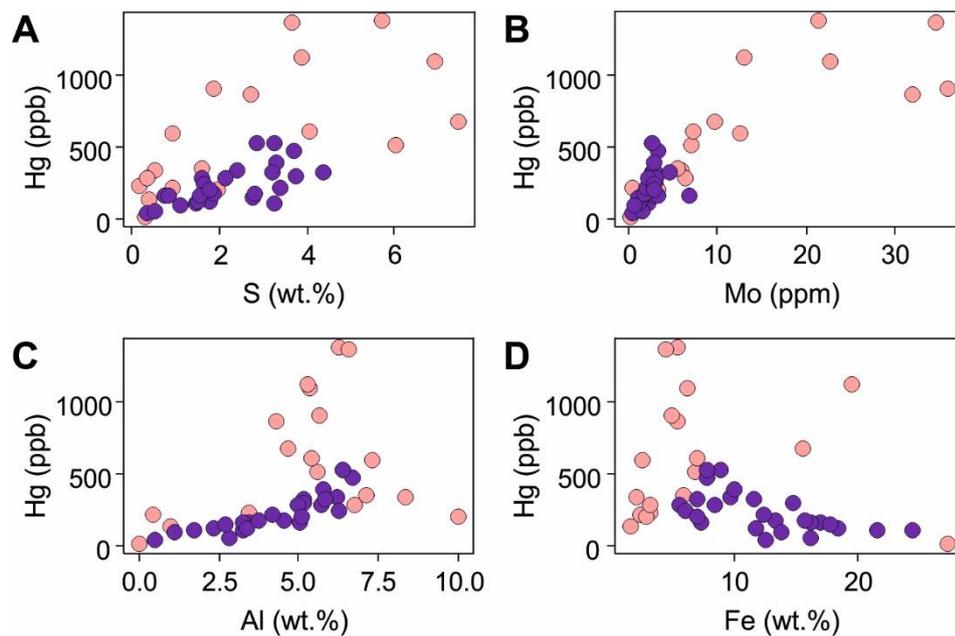
Figure S3. Cross plots of selected diagnostic elements with Hg. Dark purple data points correspond to the lower interval from 180 to 160 m stratigraphic depth, pink data points represent the upper interval above 160 m and include the 'whiff of oxygen'.